Inorganic Chemistry

Article

pubs.acs.org/IC

New Dicarboxylic Acid Bipyridine Ligand for Ruthenium Polypyridyl Sensitization of TiO_2

William B. Heuer,*[,†] Hai-Long Xia,[‡] William Ward,[‡] Zhen Zhou,[‡] Wayne H. Pearson,[†] Maxime A. Siegler,[‡] Amy A. Narducci Sarjeant,[‡] Maria Abrahamsson,*[,‡,§] and Gerald J. Meyer*[,‡]

[†]Chemistry Department, United States Naval Academy, Annapolis, Maryland 21402, United States

[‡]Department of Chemistry and Department of Materials Science and Engineering, Johns Hopkins University, 3400 North Charles Street, Baltimore, Maryland 21218, United States

[§]Department of Chemical and Biological Engineering, Chalmers University of Technology, Gothenburg, Sweden SE-412 96

Supporting Information

ABSTRACT: An ambidentate dicarboxylic acid bipyridine ligand, (4,5-diazafluoren-9-ylidene) malonic acid (dfm), was synthesized for coordination to Ru(II) and mesoporous nanocrystalline (anatase) TiO_2 thin films. The dfm ligand provides a conjugated pathway from the pyridyl rings to the carbonyl carbons of the carboxylic acid groups. X-ray crystal structures of $[Ru(bpy)_2(dfm)]Cl_2$ and the corresponding diethyl ester compound, $[Ru(bpy)_2(defm)](PF_6)_2$, were obtained. The compounds displayed intense metal-to-ligand charge transfer (MLCT) absorption bands in the visible region (ε > 11,000 M^{-1} cm^{-1} for $[Ru(bpy)_2(dfm)](PF_6)_2$ in acetonitrile). Significant room temperature photoluminescence, PL, was absent in CH_3CN but was observed at 77 K in a 4:1 EtOH:MeOH (v:v) glass. Cyclic voltammetry measurements revealed quasi-reversible $Ru^{III/II}$ electrochemistry. Ligand reductions were quasi-reversible for the diethyl ester compound $[Ru(bpy)_2(defm)]^{2+}$, but were irreversible for $[Ru(bpy)_2(dfm)]^{2+}$. Both compounds were anchored to TiO_2 thin films by overnight reactions in CH_3CN to yield saturation surface coverages of 3×10^{-8} mol/cm^2. Attenuated total reflection infrared measurements revealed that the $[Ru(bpy)_2(dfm)]^{2+}$ compound was present in the deprotonated carboxylate form when anchored to the TiO_2 surface. The MLCT excited states of both compounds injected electrons into TiO_2 with quantum yields of 0.70 in 0.1 M $LiClO_4$ CH_3CN. Micro- to milli- second charge recombination yielded ground state products. In regenerative solar cells with 0.5 M LiI/0.05 M I_2 in CH_3CN, the $Ru(bpy)_2(dfm)/TiO_2$ displayed incident photon-to-current efficiencies of 0.7 at the absorption maximum. Under the same conditions, the diethylester compound was found to rapidly desorb from the TiO_2 surface.

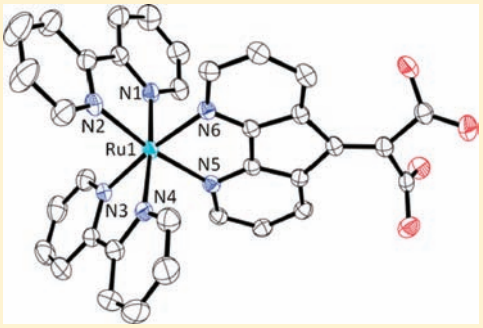

INTRODUCTION

Over thirty years ago, Goodenough and co-workers reported the use of 4,4′-$(CO_2H)_2$-2,2′-bipyridine, dcb, as an ambidentate ligand for coordination to Ru^{II} and metal oxide semiconductors.[1] To this day dcb remains the most efficient and widely utilized ligand for applications in dye sensitized solar cells.[2] The t_2-orbital parentage of the TiO_2 conduction band was expected to bond strongly with the π^* orbitals of ruthenium bipyridine excited state through carboxylic-acid derived surface linkages, but not for SnO_2 that has a conduction band orthogonal to the π^* system.[1] There now exists some experimental evidence that supports this proposal. Strong electronic coupling between the metal-to-ligand charge transfer (MLCT) excited states of dcb-containing Ru compounds and TiO_2 has been inferred from femtosecond transient absorption spectroscopy,[3] and the rate constants abstracted from such data are more rapid than those measured at SnO_2 interfaces.[4,5]

However, ultrafast measurements usually show evidence for slower picosecond components[4] to excited state injection that are detrimental for short-lived MLCT excited states, like those of iron diimine compounds,[6−8] and for driving reactions from upper excited states relevant to exceeding the well-known Schockley−Queisser limit.[9] While the origin of the slower injection processes remains speculative, experimental studies have suggested that surface heterogeneity[10] and/or interligand hopping contribute to the complex kinetics.[11] Theoretical calculations indicate that a coplanar arrangement of the carboxyl and the pyridine ring is most optimal for excited state injection; the interfacial electronic interactions decrease markedly when the carboxyl group becomes orthogonal to the pyridine ring.[12] This suggests that ultrafast injection occurs from those excited states where the carboxyl and pyridine ring are coplanar, and slower injection from those that deviate from planarity.

Here we describe a new bipyridine ligand (dfm) with a dicarboxylic acid group conjugated to the pyridine rings through an olefin group, Scheme 1. Conjugated linkers to carboxylic acid functional groups have previously been employed for

Received: July 8, 2011
Published: February 22, 2012

   dx.doi.org/10.1021/ic201395q | *Inorg. Chem.* 2012, 51, 3981−3988

Scheme 1

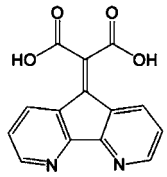

dfm

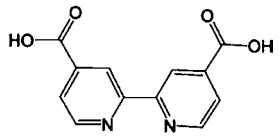

dcb

Ru(II) coordination compounds. Most notable are the "rigid rod" linkers based on oligophenyleneethynylene spacers between carboxylic acid functional groups and the pyridine rings of bipyridine.[13] However, it is well-known that rotation about the phenyl-ethyne bond dramatically alters electronic coupling much like that proposed above for excited state injection. In contrast, the sp^2 hybridization of the olefin linker in dfm prevents rotation and ensures a planar orientation of the olefin spacer with the pyridine rings. In addition, closely related malonic acid binding groups have been utilized to functionalize a variety of metal oxide surfaces with molecular compounds.[14−17] The 3,3′ bridge that connects the two pyridine rings in the dfm ligand resulted in long Ru−N_{dfm} bond lengths that had the undersirable effect of stabilizing ligand field excited states. Nevertheless, transient absorbance excited state injection yields and photocurrent measurements with a ruthenium compound based on this ligand indicate nearly quantitative excited state injection yields.

EXPERIMENTAL SECTION

Materials. All chemicals were reagent grade or better unless otherwise specified and were used without further purification. The following reagents and substrates were used as received from the indicated commercial suppliers: ruthenium(III) chloride hydrate (Aldrich); potassium thiocyanate (Acros); acetonitrile (Burdick & Jackson, spectrophotometric grade); toluene (OmniSolv, 99.99%); lithium perchlorate (Aldrich, 99.99%); *n*-tetrabutylammonium perchlorate (TBAP; Fluka, > 99.9%); argon gas (Airgas, > 99.998%); nitrogen gas (Airgas, > 99.999%); oxygen gas (Airgas, industrial grade); titanium(IV) isopropoxide (Sigma−Aldrich, 97%); fluorine-doped SnO_2-coated glass (FTO; Hartford Glass Co., Inc., 2.3 mm thick, 15 Ohm/□); and microscope slides (Fisher Scientific, 1 mm thick).

Synthesis. Diethyl(4,5-diazafluoren-9-ylidene) malonate (defm) was prepared as described previously.[18] The (4,5-diazafluoren-9-ylidene) malonic acid (dfm) ligand was isolated as the lithium carboxylate salt from hydrolysis of the diethyl ester compound, defm. Briefly, approximately 3 mmol of the diester ligand dissolved in 50 mL of acetone was added to 19 mmol LiOH in 30 mL of water at room temperature. The reaction was stirred and allowed to proceed for 5 h at which time a white solid was filtered, washed with acetone, and then dried in vacuum overnight. The crude product was recrystallized from water with acetone. ^{1}H NMR (400 MHz, D_2O): 8.43 (dd, 2H); 8.16 (dd, 2H); 7.32 (dd, 2H).

[Ru(bpy)$_2$(dfm)]Cl$_2$·6.75H$_2$O. [Ru(bpy)$_2$]Cl$_2$ (0.30 g, 0.58 mmol) and dilithium (4,5-diazafluoren-9-ylidene) malonate (0.20 g, 0.71 mmol) were dissolved in 6 mL of water with stirring. A 1 M HCl solution was then added dropwise until the stirred solution tested weakly acidic. Thirty milliliters of ethanol were then added, and the flask purged briefly with Ar. After refluxing for 12 h under Ar, the reaction mixture was filtered by gravity and taken to dryness. The solid residues were suspended in about 35 mL of 0.50 M HCl solution, heated and stirred to dissolve, and then the mixture was filtered. The filtrate was set aside to concentrate by slow evaporation for several days. Resulting crystalline solids were collected by suction filtration, washed with a small amount of 0.5 M HCl and then diethyl ether. Yield: 390 mg (90%). ^{1}H NMR (400 MHz, DMSO-d_6): 8.83 (m, 4H), 8.32 (dd, 2H), 8.15 (m, 4H), 8.05 (m, 2H), 7.81 (m, 2H), 7.63 (m, 2H), 7.59 (m, 2H), 7.52 (m, 4H). Elemental analysis: Anal. Calcd for RuC34H37.5O10.75N6Cl2: C, 46.71; H, 4.32; N, 9.61; Cl, 8.11. Found: C, 46.91; H, 3.97; N, 9.63; Cl, 8.25.

[Ru(bpy)$_2$(dfm)]Cl$_2$·3CH$_3$OH. Crystals of the methanol solvate suitable for X-ray measurements were obtained by slow diffusion of diethyl ether into 2−3 mL concentrated methanol solution of the above product.

[Ru(bpy)$_2$(defm)](PF$_6$)$_2$·CH$_3$CN. A 0.26 g portion (0.5 mmol) of [Ru(bpy)$_2$]Cl$_2$·2H$_2$O and 0.18 g (0.58 mmol) of defm were placed in a 50 mL RB flask with 25 mL of ethanol and refluxed 7 h under Ar. After cooling to room temperature, the mixture was filtered by gravity, and the filtrate was taken to dryness. The residue was taken up in minimum volume of water and loaded onto a column of Sephadex SP-C25. The column was eluted first with water, then with aqueous HCl in a concentration gradient ranging from 0.1 to 0.4 M. A pale orange component eluted first, followed by main dark red component. Collected fractions were analyzed using UV−vis. Middle fractions with similar spectra were collected together and concentrated by rotary evaporation. Saturated NH_4PF_6 solution was added to precipitate the product. After cooling at 0 °C overnight, solids were collected by centrifugation, and the supernatant was decanted. The solids were washed 2× with water and dried overnight in vacuuo. Yield: 350 mg (89%). The product was further purified by recrystallization from CH_3CN/Et_2O. ^{1}H NMR (400 MHz, CD_3CN): 8.45 (dd, 4H), 8.28 (d, 2H), 8.03 (m, 6H), 7.82 (d, 2H), 7.54 (d, 2H), 7.40 (m, 6H), 4.44 (q, 4H), 1.33 (t, 6H). Elemental Analysis: Anal. Calcd for RuC40H35O4N7P2F12: C, 44.95; H, 3.30; N, 9.17; Found: C, 44.77; H, 3.31; N, 9.00.

The crystal used for the X-ray structure determination was obtained by recrystallization from CH_3CN/Et_2O; however, no CH_3CN was located in the crystal structure. Evidently, solvent is weakly bound within the crystals and is lost upon standing in air for several weeks without disrupting the crystalline structure.

Sensitized Metal-Oxide Thin Film Electrodes. Transparent TiO_2 nanocrystallites (anatase, ∼ 15 nm in diameter) were prepared by hydrolysis of the Ti(*i*-OPr)$_4$ using a sol−gel technique previously described in the literature.[19] The sols were cast as mesoporous thin films (∼ 10 μm thick) by doctor blading onto glass microscope slides for spectroscopic measurements, transparent FTO conductive substrates for electrochemical measurements, and microscope slides for transmission-mode spectroscopic measurements. Scotch tape was employed as a spacer. In all cases, the thin films were annealed at 420 °C for 30 min under O_2 flow.

Sensitization was achieved by immersing the supported thin films in sensitizer acetonitrile solutions (μM concentrations) overnight. Films were then soaked in the neat CH_3CN for 5−10 min followed by a thorough washing with the experimental solvent. Unless noted otherwise, the thin films were sensitized to roughly maximum surface coverage, $\Gamma \sim 3 \times 10^{-8}$ mol/cm^2, which was calculated by a modified Beer−Lambert Law formula: $A = \varepsilon \times \Gamma \times 1000$. The samples were then quickly transferred to a standard 1 cm square quartz cuvette containing the experimental solution and were positioned diagonally (for microscope slide-supported films) or parallel (for FTO-supported films) in the cuvette. For at least 30 min prior to transient absorption and electrochemical studies, the cuvettes containing the sample and electrolyte solution were purged with Ar gas which was premoistened with the same electrolyte solution.

Spectroscopy. *UV−Visible Absorption.* Steady-state UV−visible (Vis) absorbance spectra were obtained on a Varian Cary 50 spectrophotometer at room temperature. Nanosecond transient absorption measurements were obtained with an apparatus similar to that which has been previously described.[20] Briefly, samples were excited by a pulsed Nd:YAG laser (Quantel U.S.A. (BigSky) Brilliant B; 5−6 ns full width at half-maximum (fwhm), 1 Hz, ∼ 10 mm in diameter) tuned to 532 nm with the appropriate nonlinear optics. The excitation fluence was measured by a thermopile power meter (Molectron) and was typically 3−4 mJ/pulse so that the absorbed fluence was typically <1 mJ/pulse, unless noted otherwise. A 150 W xenon

dx.doi.org/10.1021/ic201395q | *Inorg. Chem.* 2012, 51, 3981−3988

arc lamp (OSRAM; Applied Photophysics) served as the probe beam and was aligned orthogonal to the laser excitation light. For detection at sub-100 microsecond time scales the lamp was pulsed with 100 V. Detection was achieved with a monochromator (Spex 1702/04 spectrometer) optically coupled to an R928 photomultiplier tube (Hamamatsu). The overall instrument response time was ~10 ns.

Photoluminescence. Corrected steady-state photoluminescence (PL) measurements were obtained with a fluorimeter (Spex Fluorolog, 1681 spectrometer, 1682 double spectrometer). PL spectra were corrected for the wavelength-dependent system detection by calibration with a traceable, 45 W tungsten–halogen irradiance-standard lamp.

Infrared Absorption. Attenuated Total Reflection (ATR) FTIR absorbance spectra were obtained using a Thermo Scientific Nicolet Nexus 670 spectrophotometer with a Golden Gate ATR accessory. The measurements were made under an N_2 atmosphere and the spectra were averaged for 256 scans with 4 cm^{-1} resolution.

Electrochemistry. A potentiostat (BAS model CV-50W or Epsilon electrochemical analyzer) was employed for measurements in a standard three-electrode arrangement with a glassy carbon working electrode, a Pt gauze counter electrode, and a $Ag/AgNO_3$ reference electrode.

RESULTS

Crystals suitable for X-ray structure determination were prepared by liquid–liquid diffusion of diethyl ether into an acetonitrile solution of $[Ru(bpy)_2(defm)](PF_6)_2$ or $[Ru(bpy)_2(dfm)]Cl_2$ with methanol, Figure 1. Crystallographic data and selected bond angles/distances are given in Tables 1 and 2, respectively.

The N(5)–Ru–N(6) angle for the dfm ligand was 82.18°, and the analogous angles, N(2)–Ru–N(1) and N(3)–Ru–N(4) for the two bpy ligands were 78.98° and 79.54°, respectively. The Ru–N(5) and Ru–N(6) distances for $[Ru(bpy)_2(dfm)]^{2+}$ were 2.113 Å and 2.107 Å, respectively, whereas the four bpy Ru–N distances were 2.063 Å, 2.051 Å, 2.045 Å, and 2.062 Å. The dihedral angles between the pyidine rings within each ligand were 4.10° and 3.55° for the two bipyridine ligands and 1.73° for dfm. The two carboxylic acid groups were not equal since the torsion angles for C(34)–C(32)–C(33)–O(1) and C(33)–C(32)–C(34)–O(4) were different (106.1° and 149.5°, respectively).

The electronic absorption spectra for $[Ru(bpy)_2(dfm)]Cl_2$ and $[Ru(bpy)_2(defm)](PF_6)_2$ in CH_3CN solution are shown in Figure 2. The expected MLCT transitions in the visible region were observed, as were the bpy-centered $\pi-\pi^*$ transitions at 285 nm. The extinction coefficient for the $[Ru(bpy)_2(dfm)]Cl_2$ compound was larger than the diester compound. The addition of 8 equiv of $HClO_4$ to the $[Ru(bpy)_2(dfm)]Cl_2/CH_3CN$ solution blue-shifted the MLCT peak by 4 nm and increased the oscillator strength of both the MLCT and the ligand based transitions while the addition of 8 equiv of triethylamine (TEA) resulted in a red shift of ~3 nm to the MLCT maximum, a decrease in oscillator strengths, and the accentuation of a shoulder at approximately 325 nm. Room temperature time-resolved PL and transient absorption measurements revealed pulse-limited responses consistent with excited state lifetimes <10 ns in fluid solution. However, in a 4:1 (v/v) EtOH:MeOH glass at 77 K, visible light excitation of $[Ru(bpy)_2(dfm)]Cl_2$ alone or with added TEA led to steady state PL. The PL spectra displayed a vibrational spacing of ~1300 cm^{-1} typical of MLCT excited states, Figure 2.[21] Both the ester and the protonated carboxylic acid forms were extremely weak emitters. Excited state decay observed after pulsed excitation of $[Ru(bpy)_2(dfm)]Cl_2$ at 77 K was nonexponential but could be fit to a biexponential kinetic model, Table 3. With added TEA, first-order kinetics were observed, τ = 5.94 μs, while the excited state lifetimes of the protonated and ester forms could not be resolved, τ < 10 ns.

Table 1. Crystallographic Data for $[Ru(bpy)_2(dfm)]Cl_2{\cdot}3CH_3OH$ and $[Ru(bpy)_2(defm)](PF_6)_2$

	$[Ru(bpy)_2(dfm)]Cl_2{\cdot}3CH_3OH$[a]	$[Ru(bpy)_2(defm)](PF_6)_2$[a]
empirical formula	C37 H36 Cl2 N6 O7 Ru[a]	C38 H32 N6 O4 P2 F12 Ru[a]
formula weight	848.69[a]	1027.71[a]
temperature (K)	110	173
wavelength (Å)	0.71073	0.71073
crystal system	monoclinic	monoclinic
space group	$P2(1)/c$	$P2(1)/c$
a (Å)	8.82563(16)	11.744(4)
b (Å)	18.6217(4)	30.697(11)
c (Å)	25.0098(4)	12.589(4)
β	95.5838(15)	113.201(9)
V (Å^3)	4090.81(13)	4171(3)
Z	4	4
D_{calc} (g/cm^3)	1.378	1.636
absorption coefficient (mm^{-1})	0.566[a]	0.554[a]
$F(000)$	1736[a]	2064[a]
crystal size (mm)	0.87 × 0.37 × 0.29	0.33 × 0.02 × 0.18
θ max for data collection (deg)	26.00	25.67
final R indices [$I > 2\sigma(I)$]	R1 = 0.0407	R1 = 0.0489
R indices (all data)	wR2 = 0.1009	wR2 = 0.1277

[a]These data are given by excluding the contribution of the unresolved residual electron density via the Squeeze program by A. L. Spek *Acta Crystallogr.* **2009**, *D65*, 148–155.

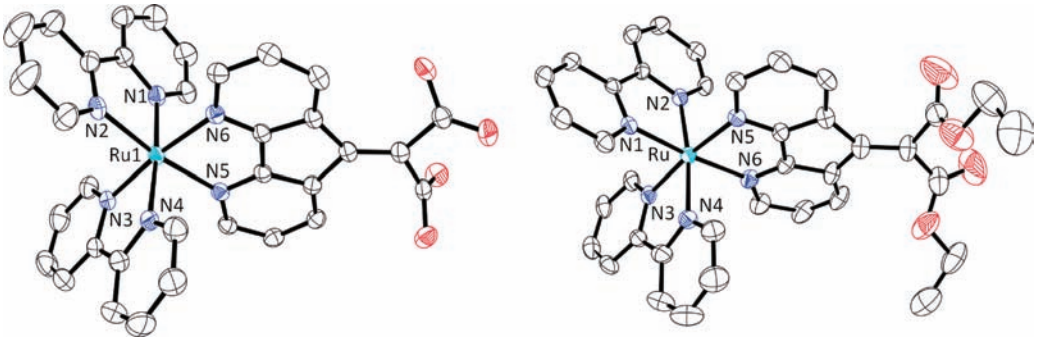

Figure 1. Displacement ellipsoid plots (50% probability level) for the cations $[Ru(bpy)_2(dfm)]^{2+}$ (left) and $[Ru(bpy)_2(defm)]^{2+}$ obtained from their respective crystal structures. H-atoms were omitted for the sake of clarity.

dx.doi.org/10.1021/ic201395q | *Inorg. Chem.* 2012, 51, 3981–3988

Table 2. Selected Bond Distances and Angles for $[Ru(bpy)_2(dfm)]Cl_2{\cdot}3CH_3OH$ and $[Ru(bpy)_2(defm)](PF_6)_2$

	$[Ru(bpy)_2(dfm)]Cl_2{\cdot}3CH_3OH$			$[Ru(bpy)_2(defm)](PF_6)_2$	
ligand	bond	distance (Å)	ligand	bond	distance (Å)
bpy-1	Ru–N(1)	2.063(2)	bpy-1	Ru–N(4)	2.066(3)
	Ru–N(2)	2.051(2)		Ru–N(3)	2.056(3)
bpy-2	Ru–N(3)	2.045(2)	bpy-2	Ru–N(1)	2.054(3)
	Ru–N(4)	2.062(2)		Ru–N(2)	2.061(3)
dfm	Ru–N(5)	2.113(2)	defm	Ru–N(5)	2.125(3)
	Ru–N(6)	2.107(2)		Ru–N(6)	2.119(3)
	$[Ru(bpy)_2(dfm)]Cl_2{\cdot}3CH_3OH$			$[Ru(bpy)_2(defm)](PF_6)_2$	
ligand	points	angle (deg)	ligand	points	angle (deg)
bpy-1	N(1)–Ru–N(2)	78.98(10)	bpy-1	N(3)–Ru–N(4)	79.17(13)
bpy-2	N(3)–Ru–N(4)	79.59(10)	bpy-2	N(1)–Ru–N(2)	79.02(12)
dfm	N(5)–Ru–N(6)	82.18(9)	defm	N(5)–Ru–N(6)	82.09(12)
	$[Ru(bpy)_2(dfm)]Cl_2{\cdot}3CH_3OH$			$[Ru(bpy)_2(defm)](PF_6)_2$	
planes		dihedral angle (deg)	planes		dihedral angle (deg)
bpy-1–bpy-2		83.24(9)	bpy-1–bpy-2		86.24(12)
bpy-1–dfm		86.80(8)	bpy-1–defm		81.23(11)
bpy-2–dfm		83.98(7)	bpy-2–defm		84.30(11)

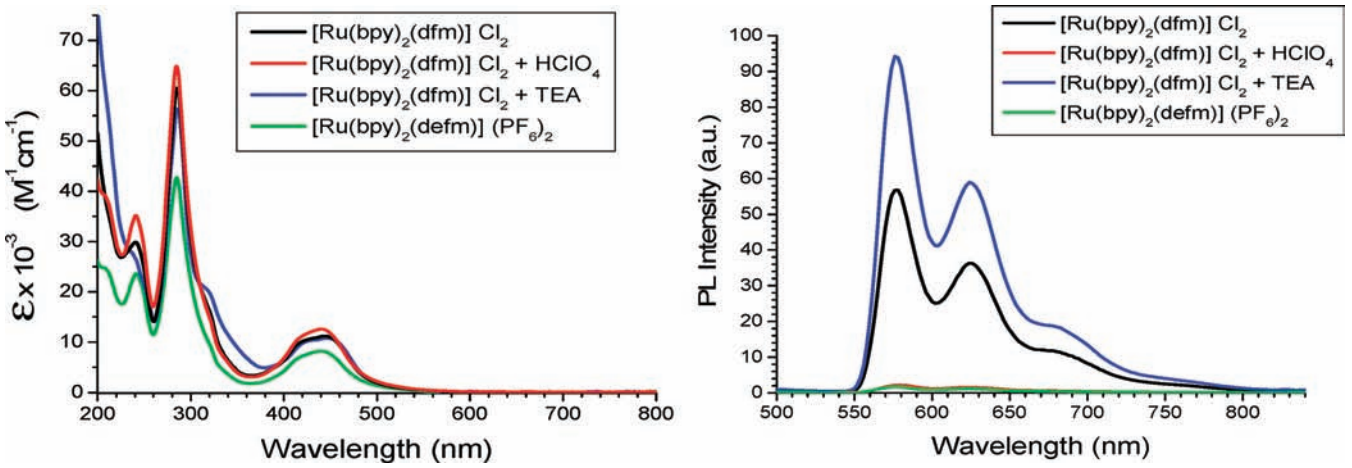

Figure 2. Room-temperature UV–visible absorption spectra in CH_3CN (left) and steady state photoluminescence spectra measured at 77 K in MeOH:EtOH glass (right), under the indicated conditions.

Cyclic voltammetry revealed a quasi-reversible Ru(III/II) redox process at positive potentials.[22] The redox chemistry was termed quasi-reversible because the anodic and cathodic currents were approximately equal, but the peak-to-peak separation was typically ~80–100 mV over scan rates of 10–100 mV/s.[25] Cathodic excursions resulted in ligand-based reductions, $E_{1/2}(Ru^{II/+})$, that were quasi-reversible for $[Ru(bpy)_2(defm)](PF_6)_2$ and irreversible for $[Ru(bpy)_2(dfm)]Cl_2$, Figure 3 and Table 3.

The compounds were anchored to TiO_2 by overnight reactions in CH_3CN. Both compounds were found to bind to TiO_2 with saturation surface coverages of 3×10^{-8} mol/cm^2, typical of Ru(II) sensitizers with a 4,4′-$(CO_2H)_2$-2,2′-bipyridine, dcb, ligand. The sensitized films are abbreviated $Ru(bpy)_2(dfm)/TiO_2$ and $Ru(bpy)_2(defm)/TiO_2$ throughout.

Attenuated total reflection Fourier transform infrared (ATR-FTIR) measurements of $[Ru(bpy)_2(dfm)]Cl_2$ showed expected bipyridine ring vibrations and an intense peak at 1710 cm^{-1} with shoulders at 1721, 1704, and 1695 cm^{-1}. When anchored to TiO_2, the absorptions in the 1695–1721 region were replaced by a broad absorption centered at 1640 cm^{-1} and a peak at 1360 cm^{-1}. The solid $[Ru(bpy)_2(defm)](PF_6)_2$ diethylester derivative showed an intense band at 1745 cm^{-1} that tailed to 1700 cm^{-1}, while intense peaks were observed at 1738 and 1731 cm^{-1} on TiO_2.

Pulsed 532 nm light excitation of $Ru(bpy)_2(dfm)/TiO_2$ or $Ru(bpy)_2(defm)/TiO_2$ thin films immersed in 0.1 M $LiClO_4$/CH_3CN resulted in the instrument response limited appearance of spectral features reasonably assigned to the oxidized sensizer and an electron injected in TiO_2, Figure 4. A bleach of the MLCT absorption band and a positive weak absorption in the red region were observed. Excited state injection yields estimated by comparative actinometry on a nanosecond time scale[23] were $\phi_{inj} = 0.70 \pm 0.05$ for both sensitized materials. The instrument response-limited appearance of this product was consistent with an excited state injection rate constant, $k_{inj} > 10^8$ s^{-1}. Recombination of the injected electron with the Ru^{III} metal center occurred quantitatively on a millisecond time scale that gave rise to absorption transients that cleanly returned to the baseline before the next laser pulse. The recombination kinetics were monitored over the first 10 microseconds where recombination was observed to be significantly faster for the dfm compound relative to the diester, Figure 4 insets.

The incident photon-to-current efficiency (IPCE) was measured in regenerative solar cells with a 0.5 M LiI/0.05 M

dx.doi.org/10.1021/ic201395q | Inorg. Chem. 2012, 51, 3981–3988

Table 3. Photophysical and Electrochemical Properties for the Ru(II) Compounds

compound	UV-Vis absorption[a] λ_{max}/nm (ε/M^{-1} cm^{-1})		PL 77 K[b] λ_{max}/nm	τ/μs
$[Ru(bpy)_2(dfm)]Cl_2$	285(60500)	444 (11200)	578	0.38, 5.31
$[Ru(bpy)_2(dfm)]Cl_2$ + $HClO_4$	285(64900)	440 (12600)		<0.01
$[Ru(bpy)_2(dfm)]Cl_2$ + TEA	286(56500)	447 (10800)	576	5.94
$[Ru(bpy)_2(defm)](PF_6)_2$	285(42700)	439 (8200)		<0.01

compound	E/V (vs $Ag/AgNO_3$)[c] $Ru^{III/II}$	reductions			
$[Ru(bpy)_2(dfm)]Cl_2$	0.92	*d*		−1.74	−1.95
$[Ru(bpy)_2(defm)](PF_6)_2$	0.96	−0.98	−1.15	−1.87	−2.12
$[Ru(bpy)_2(dafo)](PF_6)_2$[e]	1.05	−0.99	−1.68	−1.88	−2.12
$[Ru(bpy)_3]^{2+}$[e]	0.94		−1.66	−1.86	−2.11

[a]Measured in acetonitrile at room temperature. [b]Measured in 4:1 EtOH:MeOH glass. [c]Measured in 0.1 M $TBAClO_4/CH_3CN$ at room temperature. [d]Irreversible reduction. [e]Data taken from ref 33.

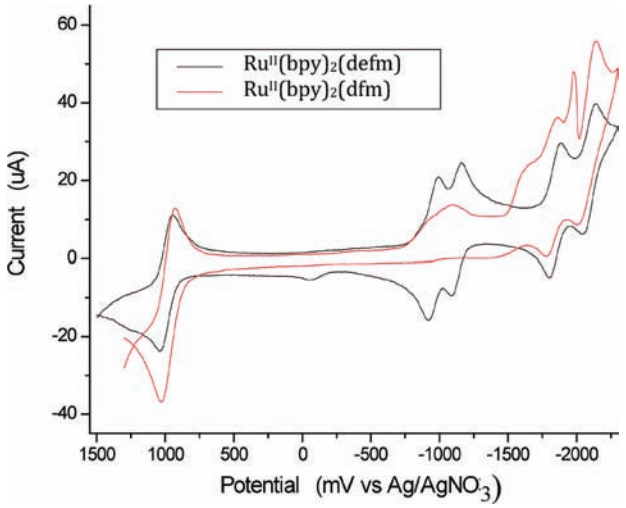

Figure 3. Cyclic voltammograms of $[Ru(bpy)_2(dfm)]Cl_2$ (red) and $[Ru(bpy)_2(defm)](PF_6)_2$ (blue) dissolved in 0.1 M $TBAP/CH_3CN$. Measurements were made at room temperature at a scan rate of 100 mV/s.

I_2/CH_3CN electrolyte. This electrolyte was found to result in significant desorption for $Ru(bpy)_2(defm)/TiO_2$ that precluded quantitative measurements. For $Ru(bpy)_2(dfm)/TiO_2$, a sustained photocurrent was observed with a photocurrent action spectrum that closely resembled the absorptance spectrum, plotted as one minus the transmittance, T, of the sensitized thin film, Figure 5. The maximum IPCE value was 0.70 ± 0.05.

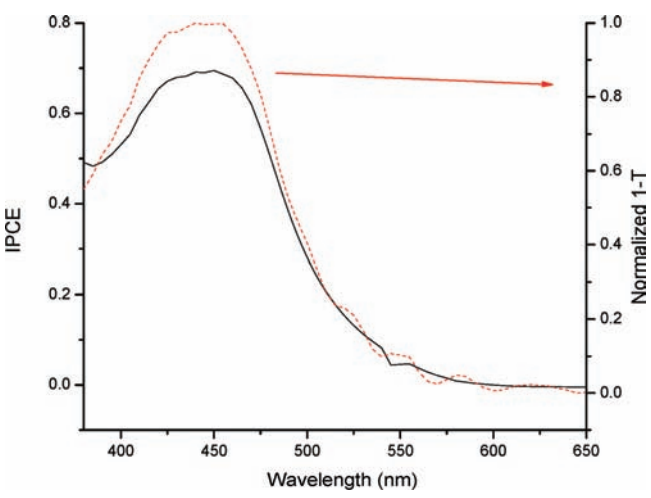

Figure 5. Incident photon to current efficiency (IPCE) and absorptance (one minus the transmittance) spectra measured for $Ru(bpy)_2(dfm)/TiO_2$ in a regenerative solar cell with a 0.5 M LiI/0.05 M I_2 acetonitrile electrolyte.

DISCUSSION

A new ambidentate ligand useful for coordination to Ru(II) and binding to a metal oxide semiconductor was synthesized, characterized, and tested. The dfm ligand provides a 2,2′-bipyridine chelate for Ru(II) with an olefin bridge in the 3 and 3′ positions to two carboxylic acid groups. The coordinated ligand dramatically decreased the lifetime of the MLCT excited states in fluid solution yet still efficiently sensitized TiO_2. In the following discussion, the MLCT excited state, redox properties, surface binding, and injection yield are described and contrasted with the widely utilized dcb ligand.

Crystallographic data for $[Ru(bpy)_2(dfm)]^{2+}$ revealed a distorted octahedral geometry around the Ru(II) metal center, with $Ru-N_{bpy}$ and $Ru-N_{dfm}$ bond lengths of about 2.050 and 2.115 Å, respectively. The elongated $Ru-N_{dfm}$ bonds are reasonably attributed to the slightly increased N−N bite angle of the dfm ligand that results from linking the two pyridine rings together. A convenient way of visualizing this is shown in Scheme 2, where the atomic coordinates from the crystal structures of $[Ru(bpy)_3]^{2+}$ and $[Ru(bpy)_2(dfm)]^{2+}$ are overlaid with the N−Ru−N atoms defining the plane of this text.

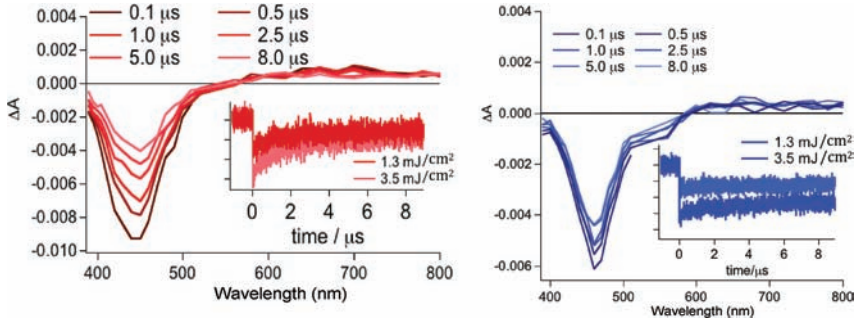

Figure 4. Absorption difference spectra measured at the indicated times after pulsed 532 nm light excitation of $Ru(bpy)_2(dfm)/TiO_2$ (left) and $Ru(bpy)_2(defm)/TiO_2$ (right). The insets display single wavelength absorption transients at the indicated irradiances.

dx.doi.org/10.1021/ic201395q | Inorg. Chem. 2012, 51, 3981−3988

Scheme 2. Ru(dfm) Overlaid on Ru(bpy) on the Left and Ru(dcb) Overlaid on Ru(bpy) on the Right

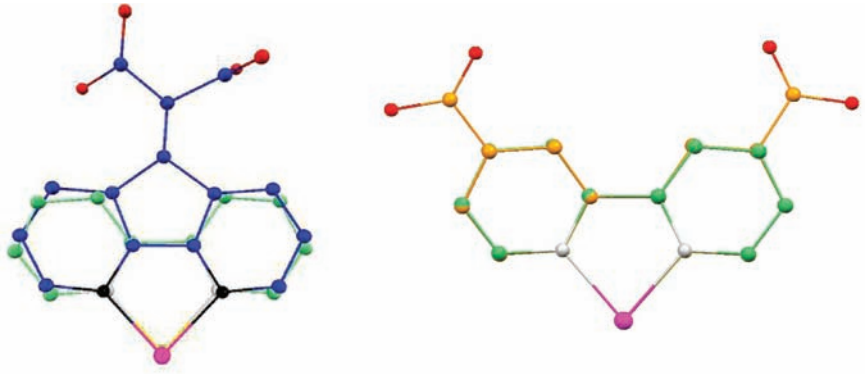

Scheme 3

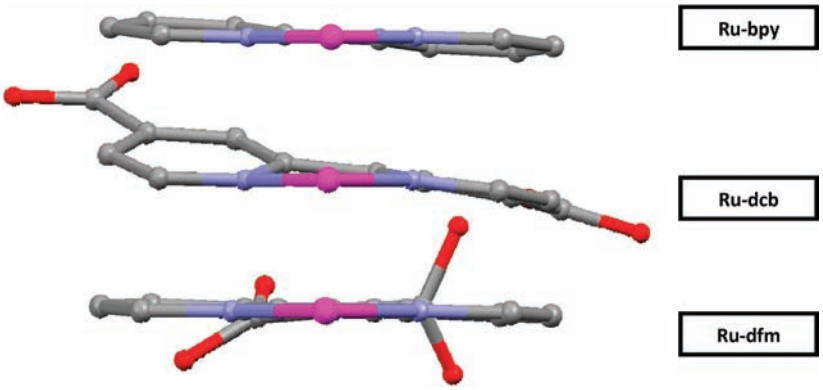

From this viewpoint, one clearly sees that the olefin group has the effect of pulling the 3 and 3′ carbons closer and hence opening the Ru bite angle by about three degrees. The elongation of the Ru−N bond that results is also observed. In contrast, when crystallographic data for $[Ru(dcb)(bpy)_2]^{2+}$ and $[Ru(bpy)_3]^{2+}$ are overlaid in the same manner, right-hand side of Scheme 2, there is no significant change evident in the bond angle or lengths. The structures are essentially superimposable. One might have anticipated that the electron withdrawing CO_2H group would influence the $Ru-N_{pyr}$ bond length. However, any inductive influence that decreases the basicity of the pyridyl nitrogens in dcb must be offset by enhanced back-bonding as there is no significant difference between dcb and bpy coordination to Ru(II) in the solid state.

Scheme 3 provides a side-on view of the Ru(bpy), Ru(dcb), and Ru(dfm) fragments taken from the crystal structures of $[Ru(bpy)_3]^{2+}$, $[Ru(bpy)_2(dcb)]^{2+}$, and $[Ru(bpy)_2(dfm)]^{2+}$, respectively. The larger dihedral angle between the two pyridine rings of dcb relative to bpy in Scheme 3 was particular to these specific compounds and was not significant in a review of 11 crystal structures of ruthenium compounds with 17 coordinated dcb ligands.[24−30] The dihedral angles ranged between 0.6 and 13 degrees for coordinated dcb and bpy ligands. The bridging olefin in the 3 and 3′ positions of dfm maintains planarity of the two pyridyl rings while a significant change in the out-of plane orientation of the oxygen atoms of the carboxylic acid groups in dfm relative to dcb was clearly observed. The oxygen atoms of the ester groups in $[Ru(bpy)_2(defm)]^{2+}$ were also significantly out of the pyridine plane.

How the solid state crystal structures are related to those when the compounds are anchored to TiO_2 and how this might influence interfacial electron transer is presently unknown. However, the influence on excited state behavior is evident. The elongated $Ru-N_{dfm}$ bond lengths measured in the solid state imply weaker bonds. Hence, 2,2′-bipyridine is expected to be a stronger field ligand than dfm. This is important as the presence of low-lying ligand field (LF) states are known to decrease MLCT excited state lifetimes and result in unwanted photochemistry.[21] Indeed, previous photophysical data reported for 3,3′-bridged bipyridyl Ru(II) compounds, based mainly on 4,5-diazafluoren-9-one (sometimes called dafo) and closely related derivatives, reveal short-lived excited states consistent with MLCT → LF internal conversion.[31−34] Both $[Ru(bpy)_2(dfm)]Cl_2$ and $[Ru(bpy)_2(defm)](PF_6)_2$ displayed no significant photoluminescence at room temperature in acetonitrile solution with excited state lifetimes <10 ns, behavior that is also reasonably assigned to MLCT excited state deactivation by low-lying LF states.

Cyclic voltammetry of $[Ru(bpy)_2(dfm)]^{2+}$ displayed an irreversible reduction while reduction of the corresponding ester compound, $[Ru(bpy)_2(defm)]^{2+}$, was reversible. Similarly, reduction of coordinated dcb ligands is irreversible while ester derivatives, such as 4,4′-$(CO_2Et)_2$-bpy, are reversible. The irreversible nature of dcb reductions has reasonably been attributed to hydrogen gas formation from the carboxylic acid protons.[35] The same may be true for $[Ru(bpy)_2(dfm)]^{2+}$. Comparisons with literature data show that the first reduction of $[Ru(bpy)_2(defm)]^{2+}$ is localized on the coordinated defm ligand. The coincidence of the irreversible reduction of $[Ru(bpy)_2(dfm)]^{2+}$ and the reversible reduction of $[Ru(bpy)_2(defm)]^{2+}$, indicates that the dfm ligand is also reduced first. For heteroleptic Ru(II) coordination compounds, DeArmond noted that

dx.doi.org/10.1021/ic201395q | Inorg. Chem. 2012, 51, 3981−3988

the first ligand reduced electrochemically was the same ligand that the excited state localizes upon in the themally equilibrated or "thexi" excited state.[36] Therefore, the relaxed MLCT excited state is reasonably formulated as $[Ru^{III}(bpy)_2(dfm^-)]^{2+*}$ and $[Ru^{III}(bpy)_2(defm^-)]^{2+*}$. The equilibrated excited state is thus expected to be localized upon the ligand that binds to TiO_2.

Infrared analysis of the surface bound sensitizers were consistent with carboxylate binding. Deacon and Philips have examined the Raman and infrared spectroscopy of X-ray crystallographically characterized metal carboxylate compounds and reported a correlation between the nature of the carboxylate-metal coordination mode and the energy separation between the antisymmetric and symmetric CO stretches, $\Delta = \nu_{assym}(CO_2^-) - \nu_{sym}(CO_2^-)$.[37] This Δ parameter has been used as an indirect measure of the surface linkage that results from the reaction of carboxylic acid containing compounds with heterogeneous metal oxide surfaces.[38−40] In this study, ATR-FTIR analysis of $Ru(bpy)_2(dfm)/TiO_2$ sensitized films yielded a $\Delta = 280\ cm^{-1}$ that is most consistent with a surface linkage where each carboxylate oxygen is linked to a single surface site, presumably Ti(IV). In previous studies of malonic acid binding to DeGussa P-25 TiO_2 particles, Dolamic and Bürgi proposed similar carboxylate binding for one of the $-CO_2$ groups with a monodentate/H-bonding mode for the other.[41] We note that DeGussa P25 is known to be a mixture of anatase and rutile TiO_2 polymorphs, and this may underlie the different binding modes observed. The vibrational spectrum of $Ru(bpy)_2(defm)/TiO_2$ showed no evidence for hydrolysis of the ester groups and the compound easily desorbed from TiO_2. Notably absent in the ATR-FTIR data of either sensitized material was any evidence for ring-opening of the central five-membered ring as had been previously noted after TiO_2 surface reactions with $[Ru(bpy)_2(dafo)]^{2+}$, where dafo is 4,5-diazofluoren-9-one.[42]

Excited state injection into TiO_2 was observed to occur with a quantum yield of 0.7 for both sensitizers on a nanosecond time scale. The incident photon-to-current efficiency also reached 0.7 in regenerative solar cells. As electron injection from ligand field states is unprecedented, subnanosecond injection from the MLCT excited state is expected. For other Ru(II) and Fe(II) compounds with low-lying ligand field states there is compelling evidence that nonradiative decay and/or spin trapping by high spin states competes kinetically with excited state injection thereby lowering the quantum yield; the observation of an excitation wavelength dependence to excited state injection was consistent with electron transfer from nonthermally equilibrated excited states.[6−8] However, in the present study, the high IPCE measured for $Ru(bpy)_2(dfm)/TiO_2$ in regenerative solar cells closely followed the absorptance spectrum of the sensitized film consistent with wavelength independent excited state injection.

CONCLUSION

A new ambidentate dicarboxylic acid ligand, dfm, that provides a continuous conjugation pathway from 2,2′-bipyridine (bpy) to a metal oxide surface was synthesisized and coordinated to $[Ru(bpy)_2]$ for sensitization of TiO_2. Even though the $[Ru(bpy)_2(dfm)]^{2+*}$ MLCT excited state lifetime was <10 ns, efficient $\phi_{inj} = 0.70 \pm 0.05$ interfacial electron transfer to TiO_2 was observed. The shortened MLCT excited state was attributed to the bridging olefin that increased the N−Ru−N bite angle in the dfm ligand thereby elongating these Ru−N bonds and stabilizing antibonding ligand field excited states. The dfm ligand provides a new alternative to the commonly utilized 4,4′-$(CO_2H)_2$-2,2′-bipyridine (dcb) ligand for the coordination of transition metal compounds to metal oxide surfaces.

ASSOCIATED CONTENT

Supporting Information

Crystallographic data in CIF format. This material is available free of charge via the Internet at http://pubs.acs.org.

AUTHOR INFORMATION

Corresponding Author

*E-mail: meyer@jhu.edu (G.J.M.).

Notes

The authors declare no competing financial interest.

ACKNOWLEDGMENTS

The National Science Foundation is gratefully acknowledged for research support, Grant CHE-091158. M.A. thanks the Swedish Research Council for a personal postdoctoral research grant, 623-2007-1038. W.B.H. acknowledges support from the Naval Academy Research Council.

REFERENCES

(1) Anderson, S.; Constable, E. C.; Dare-Edwards, M. P.; Goodenough, J. B.; Hamnett, A.; Seddon, K. R.; Wright, R. D. *Nature* **1979**, *280*, 571−573.
(2) O'Regan, B.; Grätzel, M. *Nature* **1991**, *353*, 737−740.
(3) Watson, D. F.; Meyer, G. J. *Annu. Rev. Phys. Chem.* **2005**, *56*, 119−156.
(4) Asbury, J. B.; Ellingson, R. J.; Ghosh, H. N.; Ferrere, S.; Nozik, A. J.; Lian, T. *J. Phys. Chem. B* **1999**, *103*, 3110−3119.
(5) Benkoe, G.; Myllyperkioe, P.; Pan, J.; Yartsev, A. P.; Sundstroem, V. *J. Am. Chem. Soc.* **2003**, *125*, 1118−1119.
(6) Ferrere, S.; Gregg, B. A. *J. Am. Chem. Soc.* **1998**, *120*, 843−844.
(7) Xia, H.-L.; Ardo, S.; Narducci Sarjeant, A. A.; Huang, S.; Meyer, G. J. *Langmuir* **2009**, *25*, 13641−13652.
(8) Yang, M.; Thompson, D. W.; Meyer, G. J. *Inorg. Chem.* **2002**, *41*, 1254−1262.
(9) Hoertz, P. G.; Staniszewski, A.; Marton, A.; Higgins, G. T.; Incarvito, C. D.; Rheingold, A. L.; Meyer, G. J. *J. Am. Chem. Soc.* **2006**, *128*, 8234−8245.
(10) Wenger, B.; Graetzel, M.; Moser, J.-E. *J. Am. Chem. Soc.* **2005**, *127*, 12150−12151.
(11) Kallioinen, J.; Benkoe, G.; Sundstroem, V.; Korppi-Tommola, J. E. I.; Yartsev, A. P. *J. Phys. Chem. B* **2002**, *106*, 4396−4404.
(12) Schnadt, J.; Schiessling, J.; O'Shea, J. N.; Gray, S. M.; Patthey, L.; Johansson, M. K. J.; Shi, M.; Krempaský, J.; Åhlund, J.; Karlsson, P. G.; Persson, P.; Mårtensson, N.; Brühwiler, P. A. *Surf. Sci.* **2003**, *540*, 39−54.
(13) Galoppini, E. *Coord. Chem. Rev.* **2004**, *248*, 1283−1297.
(14) Campbell, W. M.; Jolley, K. W.; Wagner, P.; Wagner, K.; Walsh, P. J.; Gordon, K. C.; Schmidt-Mende, L.; Nazeeruddin, M. K.; Wang, Q.; Graetzel, M.; Officer, D. L. *J. Phys. Chem. C* **2007**, *111*, 11760−11762.
(15) Wang, P.; Zakeeruddin, S. M.; Comte, P.; Charvet, R.; Humphry-Baker, R.; Graetzel, M. *J. Phys. Chem. B* **2003**, *107*, 14336−14341.
(16) Hoertz, P. G.; Kim, Y.-I.; Youngblood, W. J.; Mallouk, T. E. *J. Phys. Chem. B* **2007**, *111*, 6845−6856.
(17) Youngblood, W. J.; Lee, S.-H. A.; Kobayashi, Y.; Hernandez-Pagan, E. A.; Hoertz, P. G.; Moore, T. A.; Moore, A. L.; Gust, D.; Mallouk, T. E. *J. Am. Chem. Soc.* **2009**, *131*, 926−927.
(18) Utley, J. H. P.; Ling-Chung, S. K. *Electrochim. Acta* **1997**, *42*, 2109−2115.
(19) Ardo, S.; Sun, Y.; Staniszewski, A.; Castellano, F. N.; Meyer, G. J. *J. Am. Chem. Soc.* **2010**, *132*, 6696−6709.

(20) Heimer, T. A.; D'Arcangelis, S. T.; Farzad, F.; Stipkala, J. M.; Meyer, G. J. *Inorg. Chem.* **1996**, *35*, 5319−5324.
(21) Kalyanasundarum, K. *Photochemistry of Polypyridine and Porphyrin Complexes*; Academic Press: New York, NY, 1992.
(22) Bard, A. J.; Faulkner, L. R. *Electrochemical Methods: Fundamentals and Applications*; Wiley Interscience: New York, 1980.
(23) Bergeron, B. V.; Kelly, C. A.; Meyer, G. J. *Langmuir* **2003**, *19*, 8389−8394.
(24) Philippopoulos, A. I.; Terzis, A.; Raptopoulou, C. P.; Catalano, V. J.; Falaras, P. *Eur. J. Inorg. Chem.* **2007**, *2007*, 5633−5644.
(25) Eskelinen, E.; Da Costa, P.; Haukka, M. *J. Electroanal. Chem.* **2005**, *579*, 257−265.
(26) Caspar, R.; Amouri, H.; Gruselle, M.; Cordier, C.; Malézieux, B.; Duval, R.; Leveque, H. *Eur. J. Inorg. Chem.* **2003**, *2003*, 499−505.
(27) Fujihara, T.; Kobayashi, A.; Iwai, M.; Nagasawa, A. *Acta Crystallogr., Sect.E: Struct.Rep.Online* **2004**, m1172.
(28) Eskelinen, E.; Luukkanen, S.; Haukka, M.; Ahlgren, M.; Pakkanen, T. A. *J. Chem. Soc., Dalton Trans.* **2000**, 2745.
(29) Homanen, P.; Haukka, M.; Ahlgraen, M.; Pakkanen, T. A. *Inorg. Chem.* **1997**, *36*, 3794−3797.
(30) Luukkanen, S.; Haukka, M.; Eskelinen, E.; Pakkanen, T. A.; Lehtovuori, V.; Kallioinen, J.; Myllyperkio, P.; Korppi-Tommola, J. *Phys. Chem. Chem. Phys.* **2001**, 1992.
(31) Henderson, L. J.; Fronczek, F. R.; Cherry, W. R. *J. Am. Chem. Soc.* **1984**, *106*, 5876−5879.
(32) Wacholtz, W. M.; Auerbach, R. A.; Schmehl, R. H.; Ollino, M.; Cherry, W. R. *Inorg. Chem.* **1985**, *24*, 1758−1760.
(33) Wang, Y.; Perez, W.; Zheng, G. Y.; Rillema, D. P. *Inorg. Chem.* **1998**, *37*, 2051−2059.
(34) Zheng, G. Y.; Wang, Y.; Rillema, D. P. *Inorg. Chem.* **1996**, *35*, 7118−7123.
(35) Wolfbauer, G.; Bond, A. M.; Deacon, G. B.; MacFarlane, D. R.; Spiccia, L. *J. Am. Chem. Soc.* **2000**, *122*, 130−142.
(36) Ohsawa, Y.; DeArmond, M. K.; Hanck, K. W.; Morris, D. E.; Whitten, D. G.; Neveux, P. E. *J. Am. Chem. Soc.* **1983**, *105*, 6522−6524.
(37) Deacon, G. B.; Phillips, R. J. *Coord. Chem. Rev.* **1980**, *33*, 227−250.
(38) Shibano, Y.; Umeyama, T.; Matano, Y.; Imahori, H. *Org. Lett.* **2007**, *9*, 1971−1974.
(39) Kilså, K.; Mayo, E. I.; Brunschwig, B. S.; Gray, H. B.; Lewis, N. S.; Winkler, J. R. *J. Phys. Chem. B* **2004**, *108*, 15640−15651.
(40) Meyer, T. J.; Meyer, G. J.; Pfennig, B. W.; Schoonover, J. R.; Timpson, C. J.; Wall, J. F.; Kobusch, C.; Chen, X.; Peek, B. M. *Inorg. Chem.* **1994**, *33*, 3952−3964.
(41) Dolamic, I.; Buergi, T. *J. Phys. Chem. B* **2006**, *110*, 14898−14904.
(42) Heuer, W. B.; Xia, H.-L.; Abrahamsson, M.; Zhou, Z.; Ardo, S.; Sarjeant, A. A. N.; Meyer, G. J. *Inorg. Chem.* **2010**, *49*, 7726−7734.